17. Steane, A. M. Error correcting codes in quantum theory. *Phys. Rev. Lett.* **77,** 793–797 (1996).
18. Gottesman, D. *Stabilizer Codes and Quantum Error Correction*. Thesis, California Inst. of Technol. (1997).
19. Boykin, P. O., More, T., Pulver, M., Roychowdhury, V. & Vatan, F. On universal and fault-tolerant quantum computing. Preprint quant-ph/9906054 (cited June 1999) at ⟨http://xxx.lanl.gov⟩ (1999).
20. Kwiat, P. G. & Weinfurter, H. Embedded Bell-state analysis. *Phys. Rev. A* **58,** R2623–R2626 (1998).
21. Bouwmeester, D. *et al*. Experimental quantum teleportation. *Nature* **390**, 575–579 (1997).
22. Bouwmeester, D. *et al*. Observation of three-photon Greenberger-Horne-Zeilinger entanglement. *Phys. Rev. Lett.* **82,** 1345–1349 (1999).
23. Chuang, I. L. & Yamamoto, Y. Simple quantum computer. *Phys. Rev. A* **52,** 3489–3496 (1995).

Acknowledgements

We thank C. Bennett for suggesting the concept of "quantum sofrware" to us, and R. Jozsa for pointing out an error in an early version of this manuscript. We also thank J. Kempe, D. Leung, and D. Bacon for helpful discussions. This work was supported in part by DARPA under the NMRQC initiative.

Correspondence and requests for materials should be addressed to I.L.C. (e-mail: ichuang@almaden.ibm.com).

Coupled synthesis and self-assembly of nanoparticles to give structures with controlled organization

Mei Li*, Heimo Schnablegger† & Stephen Mann*

* *School of Chemistry, University of Bristol, Bristol BS8 1TS, UK*
† *Max-Planck-Institut of Colloids and Interfaces, Am Muehlenberg, D-14476 Golm, Germany*

Colloidal inorganic nanoparticles have size-dependent optical, optoelectronic and material properties that are expected to lead to superstructures with a range of practical applications[1,2]. Discrete nanoparticles with controlled chemical composition and size distribution are readily synthesized using reverse micelles and microemulsions as confined reaction media[3–5], but their assembly into well-defined superstructures amenable to practical use remains a difficult and demanding task. This usually requires the initial synthesis of spherical nanoparticles, followed by further processing such as solvent evaporation[6–8], molecular cross-linking[9–14] or template-patterning[15–18]. Here we report that the interfacial activity of reverse micelles and microemulsions can be exploited to couple nanoparticle synthesis and self-assembly over a range of length scales to produce materials with complex organization arising from the interdigitation of surfactant molecules attached to specific nanoparticle crystal faces. We demonstrate this principle by producing three different barium chromate nanostructures—linear chains, rectangular superlattices and long filaments—as a function of reactant molar ratio, which in turn is controlled by fusing reverse micelles and microemulsion droplets containing fixed concentrations of barium and chromate ions, respectively. If suitable soluble precursors and amphiphiles with headgroups complementary to the crystal surface of the nanoparticle target are available, it should be possible to extend our approach to the facile production of one-dimensional 'wires' and higher-order colloidal architectures made of metals and semiconductors.

Barium bis(2-ethylhexyl)sulphosuccinate ($Ba(AOT)_2$) reverse micelles were added to sodium chromate (Na_2CrO_4)-containing NaAOT microemulsion droplets, to give final molar ratios of $[Ba^{2+}] : [CrO_4^{2-}] \approx 1$ and water content $w = [H_2O] : [NaAOT] = 10$. This produced a yellow precipitate ~3 h after addition of the reactants at 25 °C. Transmission electron microscopy (TEM) images of samples taken directly from the liquid phase of the microemulsion showed chain-like arrays that contained up to 60 nanoparticles (Fig. 1). The colloidal chain structures were 50–500 nm in length and consisted of rectangular-shaped particles that were uniform in length (mean = 16.0 ± 1.5 nm) and width (mean = 6.0 ± 0.4 nm), and preferentially aligned so that the long axis of each particle was perpendicular to the chain direction. Energy dispersive X-ray analysis and powder electron diffraction patterns indicated that the nanoparticles were crystalline $BaCrO_4$ with an orthorhombic unit cell ($a = 0.911$, $b = 0.554$, $c = 0.734$ nm). Each crystal along the length of the chain was separated by a regular spacing of 2 nm, consistent with the presence of an interdigitated layer of surfactant molecules.

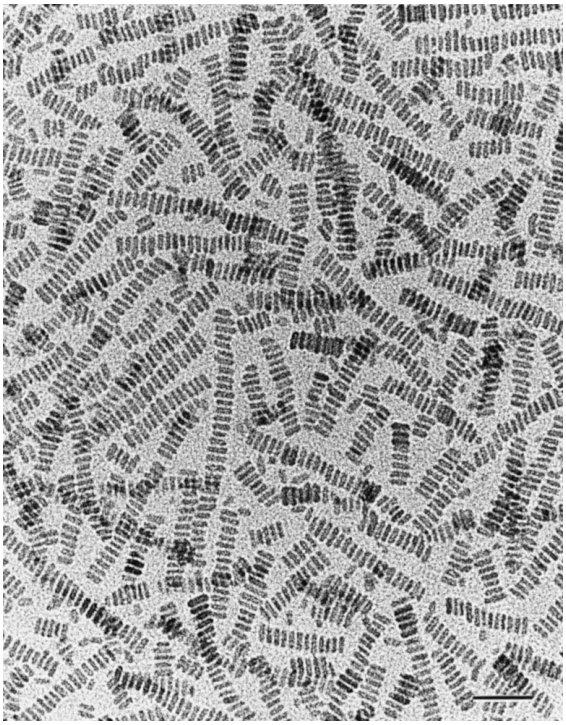

Figure 1 TEM image showing ordered chains of prismatic $BaCrO_4$ nanoparticles. The nanoparticles were prepared in AOT microemulsions at $[Ba^{2+}] : [CrO_4^{2-}]$ molar ratio ≈1 and $w = 10$. Scale bar = 50 nm.

Corresponding TEM studies on the sedimented material showed thin flake-like aggregates of a two-dimensional superlattice constructed from a pseudo-rectangular ($90° \leqslant \theta \leqslant 100°$) array of uniformly sized $BaCrO_4$ nanoparticles that were separated by an interparticle spacing of 2 nm (Fig. 2). Thermal analysis indicated that the superlattices contained ~30% by weight of surfactant. Images of tilted lattices indicated that the particles were prismatic and identical to those present in the chain motif, and aligned with their long axis perpendicular to the plane of the superlattice. Viewed in-plane, the nanoparticles were rectangular in shape with mean dimensions of 6.8 ± 0.6 nm and 5.9 ± 0.5 nm, indicating two different types of side face. Electron diffraction failed to identify unequivocally the crystallographic nature of the side faces because of multiple arcing of the reflections arising from long-range disorder in the air-dried structures. However, patterns recorded from particles in the superlattice structure were indexed according to a superimposition of directions close to the [100] zone axis, which indicated that the prismatic crystals were single-domain particles elongated along the crystallographic *a* axis. This was consistent with a morphology based on a set of {100} end faces with {010} and {001} side faces.

Systematic changes in the water content ($5 \leqslant w \leqslant 20$), and hence

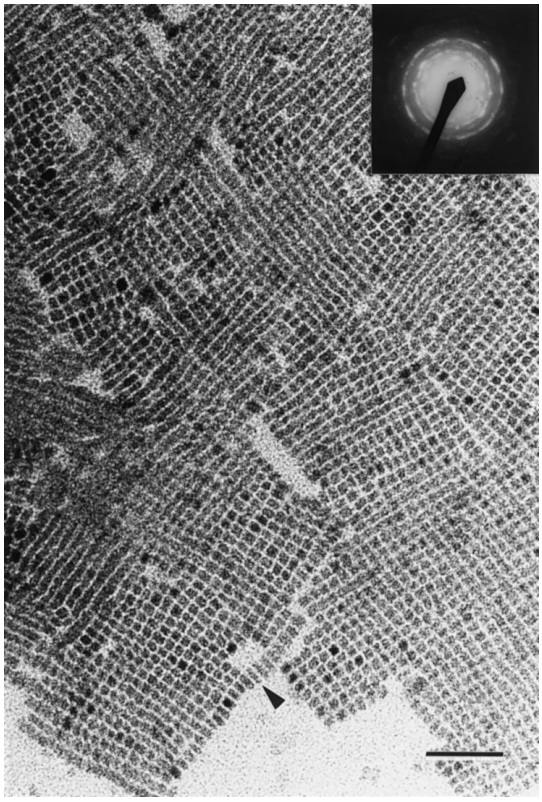

Figure 2 Rectangular superlattice of $BaCrO_4$ nanoparticles. These were formed by two-dimensional aggregation of nanoparticle chains prepared in AOT microemulsions at $[Ba^{2+}]:[CrO_4^{2-}]$ molar ratio ≈1 and $w = 10$. Arrow shows dislodged particles revealing the prismatic morphology of individual crystallites. Scale bar = 50 nm. Inset, the electron diffraction pattern gives the superimposition of reflections from zone axes approximately parallel to the [100] direction.

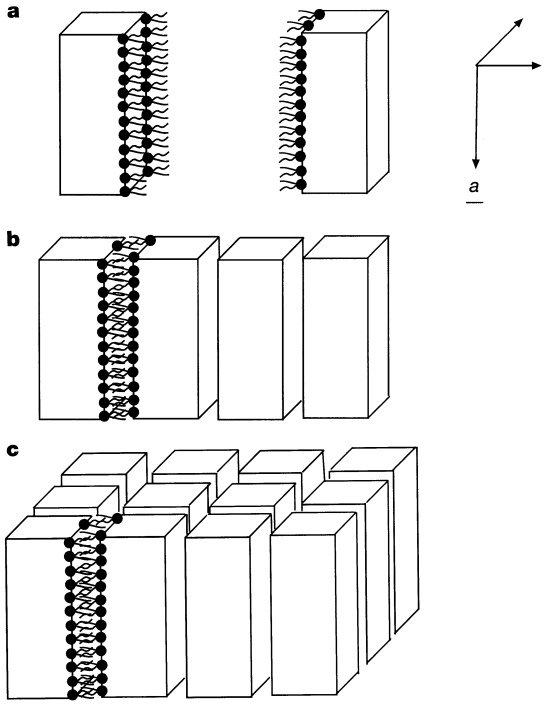

Figure 3 Proposed model for the surfactant-induced self-assembly of nanoparticle chains and superlattices. **a**, Surfactant-coated prismatic $BaCrO_4$ nanoparticles synthesized by controlled crystallization in microemulsion water droplets. For clarity, only one face is shown with associated surfactant molecules. **b**, Interdigitation of the surfactant monolayers induced as the crystal faces develop in shape and size, resulting in preferential aggregation normal to both the prism long axis (crystallographic *a* axis) and largest side face. **c**, Aggregation in two dimensions proceeds as the chains develop in length and number.

in the diameter of the microemulsion droplets, was used to control the size of the nanoparticles present in both the chain and superlattice structures. For constant values of $[Ba^{2+}] : [CrO_4^{2-}] \approx 1$, increases in w gave increased mean particle sizes that were correlated in the chain and superlattice nanostructures (Table 1). The particle width measured for crystals in the individual chains was commensurate with the shorter in-plane dimension of the superlattice particles, suggesting that the larger side faces were preferentially juxtaposed in the stacked linear array.

Dynamic light-scattering (DLS) of unstirred microemulsions, prepared as above at $w = 10$, suggested the presence of microemulsion water droplets with a constant hydrodynamic radius of 5.8 ± 0.5 nm throughout the time course of the experiments. Similar observations were made using small-angle X-ray scattering (SAXS), which detected significant numbers of Ba^{2+}-containing spherical water droplets in the reaction mixtures, even after 25 h at 25 °C. DLS also suggested the appearance of a second component within 3 hours at 25 °C (or 18 h at 20 °C), which progressively increased in scattering intensity over 6 h at 25 °C, until the experiment was terminated due to bulk precipitation. Although the complexity of the system must prevent a conclusive analysis of the DLS data, they do suggest that the second component is associated with the formation of aggregates in the microemulsion fluid. Supporting this interpretation are the results of a TEM analysis of corresponding samples, which show the appearance of the second component in the DLS studies to be concurrent with the appearance of nanoparticle chains. Taken together, the data suggest that spontaneous self-assembly of the $BaCrO_4$ linear arrays occurs in the microemulsion fluid.

TEM images of the initial stages of chain assembly showed low-contrast structures with striped patterns, rather than isolated nanoparticles with prismatic morphology, suggesting that $BaCrO_4$ growth occurs in association and concurrent with the self-organization of stacked micellar aggregates and not through sequential attachment of individual nanoparticles. One possibility is that the linear arrays spontaneously self-assemble in the microemulsion fluid from interactions between the hydrophobic tails of AOT molecules absorbed onto the flat side faces of developing $BaCrO_4$ prismatic crystallites (Fig. 3). A difference of only ~14 nm^2 in the surface areas of the two sets of side faces appears to be sufficient to stabilize the chain motif before superlattice formation, even though the latter has an increased number of particle–particle connections.

The $BaCrO_4$ nanoparticle chains and superlattices were formed specifically at molar equivalence $(1 : 1.4 \leqslant [Ba^{2+}] : [CrO_4^{2-}] \leqslant 1.4 : 1)$. Under identical conditions, but with an excess of Ba^{2+}

Table 1 Mean dimensions for individual prismatic $BaCrO_4$ nanoparticles

w value (H_2O/NaAOT)	Chain-like stacks (nm)	Superlattices (nm)	Microemulsion radius (nm)
5	14.5 ± 1.2 × 5.6 ± 0.4	6.4 ± 0.6 × 5.3 ± 0.5	1.5 ± 0.5
10	16.0 ± 1.5 × 6.0 ± 0.4	6.8 ± 0.6 × 5.9 ± 0.5	2.2 ± 0.6
15	17.5 ± 1.4 × 6.3 ± 0.4	7.4 ± 0.7 × 6.1 ± 0.6	–
20	18.3 ± 1.5 × 8.4 ± 0.8	10.0 ± 1.1 × 8.1 ± 0.7	3.2 ± 0.6

The nanoparticles were viewed side-on (chains) and end-on (superlattice) by electron microscopy. The nanostructures were synthesized in AOT/water/isooctane reverse microemulsions at $[Ba^{2+}] : [CrO_4^{2-}] \approx 1 : 1$, [NaAOT] : $[Ba(AOT)_2] = 50$, and various water content *w* values. Sizes of the corresponding microemulsion water droplets were determined by small-angle X-ray scattering. $\sigma < 10\%$ for all data.

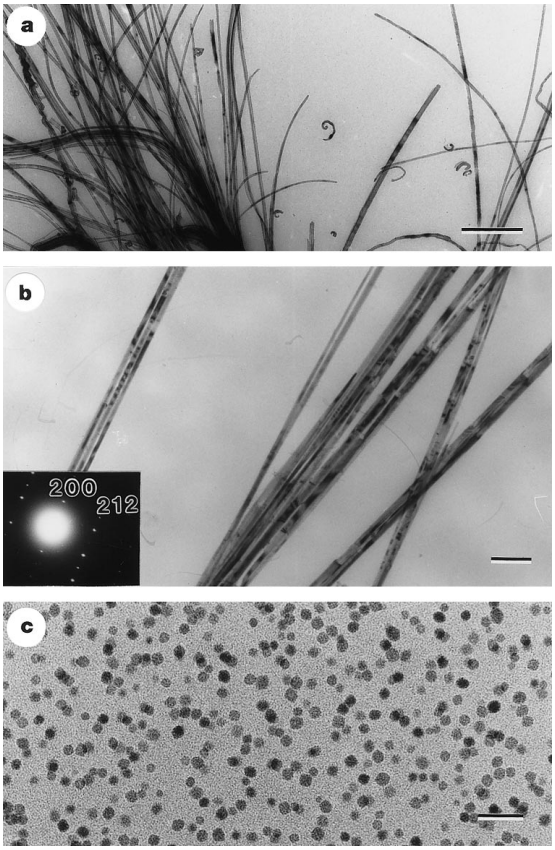

Figure 4 Characterization of $BaCrO_4$ nanostructures formed at different reactant ratios. **a**, TEM image of bundles of $BaCrO_4$ nanofilaments prepared in AOT microemulsions at $[Ba^{2+}] : [CrO_4^{2-}] \approx 5 : 1$ and $w = 10$; scale bar = 500 nm. **b**, Higher magnification image of single filaments elongated along the crystallographic *a* axis; scale bar = 200 nm. Inset, $[0\bar{2}1]$ zone electron diffraction pattern recorded from an individual fibre. **c**, Spherical $BaCrO_4$ nanoparticles prepared at $[Ba^{2+}] : [CrO_4^{2-}] \approx 1 : 5$ and $w = 10$; scale bar = 50 nm.

$(2.7 : 1 \leqslant [Ba^{2+}] : [CrO_4^{2-}] \leqslant 5.5 : 1)$, $BaCrO_4$ filaments with lengths up to 50 μm were deposited in the form of single threads or bundles of loosely aggregated fibres with highly uniform widths, straight edges and well-defined flattened ends (Fig. 4a and b). Similar structures have been reported for $BaSO_4$ crystallization in microemulsions[19]. The filaments were 20–500 nm in width, with an aspect ratio of approximately 1,000. Electron diffraction patterns and lattice images were consistent with single-crystal $BaCrO_4$ filaments preferentially oriented along the crystallographic *a* axis. In contrast, when a molar excess of chromate was used $(1 : 4.6 \leqslant [Ba^{2+}] : [CrO_4^{2-}] \leqslant 1 : 2.7)$, no precipitate was observed, and TEM studies showed that the colloidal suspension consisted of cuboidal and spherical $BaCrO_4$ nanocrystals with a mean size of 11.1 ± 2.5 nm (Fig. 4c). When experiments were undertaken at these increased chromate concentrations but with the molar ratio re-established at 1 : 1 by increasing the $Ba(AOT)_2$ concentration, chains and superlattices, and not discrete spherical nanoparticles, were specifically deposited. This confirmed that the molar ratio, rather than the absolute concentrations, was responsible for the organized structures.

We suggest that on mixing, transfer of water molecules from the chromate-containing microemulsions to the 'dry' $Ba(AOT)_2$ reverse micelles acts as a strong driving force for the exchange of ions, which results in an increase in intramicellar supersaturation, and nucleation and growth of surfactant-encapsulated $BaCrO_4$ crystals. At molar equivalence, there is no net charge at the crystal surfaces, so that the particles develop regular faces and a prismatic morphology in accordance with the unit cell symmetry, and aggregate into ordered chains by the mechanism proposed in Fig. 3. In contrast, a molar excess of CrO_4^{2-} offsets the growth anisotropy, owing to excess negative surface charge, to produce spherical nanoparticles. The AOT molecules are also negatively charged, so there is negligible interaction (adsorption) with the particle surface, and therefore no driving force for surfactant-induced aggregation into longer range structures. An excess of Ba^{2+} ions, on the other hand, results in highly positively charged clusters that interact with the AOT headgroups to such an extent that further growth into regularly shaped nanoparticles is inhibited. Instead, large unstructured micellar aggregates are formed which precipitate from solution and slowly transform over a period of days and weeks into filamentous structures (M.L. and S.M., unpublished data). □

Methods

Sodium AOT was converted to $Ba(AOT)_2$ by direct precipitation as described elsewhere[19]. The following procedure was used for the synthesis of $BaCrO_4$ within microemulsions. Typically, 0.18 ml of aqueous Na_2CrO_4 solution (0.02–0.50 M, pH ≈ 9) were added with shaking to 10 ml of a solution of NaAOT dissolved in isooctane (0.1 M) to give yellow suspensions of microemulsion droplets with water to surfactant molar ratio $w = [H_2O] : [NaAOT] = 10$. To introduce Ba^{2+} ions into the reaction, a small amount of $Ba(AOT)_2$ dissolved in isooctane (0.395 ml, 0.05 M, $w < 1$) was added to 10 ml of the chromate-containing microemulsion to give a final NaAOT : $Ba(AOT)_2$ molar ratio of 50 : 1. Under these conditions, the $[Ba^{2+}] : [CrO_4^{2-}]$ molar ratio was systematically changed between values of 5.5 : 1 to 1 : 4.6 by modifying the concentration of Na_2CrO_4 in the microemulsion water droplets. Samples for TEM were collected within one week directly from the microemulsion fluid as well as the precipitated material, and air-dried and washed with pure isooctane on the TEM grids.

Received 20 April; accepted 21 October 1999.

1. Petit, C., Taleb, A. & Pileni, M. P. Self-organization of magnetic nanosized cobalt particles. *Adv. Mater.* **10,** 259–261 (1998).
2. Taleb, A., Petit, C. & Pileni, M. P. Optical properties of self-assembled 2D and 3D superlattices of silver nanoparticles. *J. Phys. Chem.* **102,** 2214–2220 (1998).
3. Taleb, A., Petit, C. & Pileni, M. P. Synthesis of highly monodisperse silver nanoparticles from AOT reverse micelles: A way to 2-D and 3-D self-organization. *Chem. Mater.* **9,** 950–959 (1997).
4. Motte, L., Billoudet, F., Lacaze, E. & Pileni, M. P. Self-organization of size-selected nanoparticles into three-dimensional superlattices. *Adv. Mater.* **8,** 1018–1020 (1996).
5. Sager, W. F. C. Controlled formation of nanoparticles from microemulsions. *Curr. Opin. Colloid Interf. Sci.* **3,** 276–283 (1998).
6. Murray, C. B., Kagan, C. R. & Bawendi, M. G. Self-organization of CdSe nanocrystals into three-dimensional quantum dot superlattices. *Science* **270,** 1335–1338 (1995).
7. Vossmeyer, T. *et al.* A double-diamond superlattice built-up of $Cd_{17}S_4(SCH_2OH)_{26}$ clusters. *Science* **267,** 1476–1479 (1995).
8. Wang, Z. L. Structural analysis of self-assembling nanocrystal superlattices. *Adv. Mater.* **10,** 13–30 (1998).
9. Andres, R. P. *et al.* Self-assembly of a two-dimensional superlattice of molecularly linked metal clusters. *Science* **273,** 1690–1693 (1996).
10. Brust, M., Bethell, D., Schiffrin, D. J. & Kiely, C. J. Novel gold-dithiol nanonetworks with non-metallic electronic properties. *Adv. Mat.* **7,** 795–797 (1995).
11. Mirkin, C. A., Letsinger, R. L., Mucic, R. C. & Storhoff, J. J. A DNA-based method for rationally assembling nanoparticles into macroscopic materials. *Nature* **382,** 607–609 (1996).
12. Alivisatos, A. P. *et al.* Organization of "nanocrystal molecules" using DNA. *Nature* **382,** 609–611 (1996).
13. Li, M., Wong, K. K. W. & Mann, S. Organization of inorganic nanoparticles using biotin-streptavidin connectors. *Chem. Mater.* **11,** 23–26 (1999).
14. Shenton, W., Davis, S. A. & Mann, S. Directed self-assembly of nanoparticles into macroscopic materials using antibody-antigen recognition. *Adv. Mater.* **11,** 449–452 (1999).
15. Shenton, W., Pum, D., Sleytr, U. B. & Mann, S. Biocrystal templating of CdS superlattices using self-assembled bacterial S-layers. *Nature* **389,** 585–587 (1998).
16. Dieluweit, S., Pum, D. & Sleytr, U. B. Formation of a gold superlattice on an S-layer with square lattice symmetry. *Supramol. Sci.* **5,** 15–19 (1998).
17. Davis, S. A., Burkett, S. L., Mendelson, N. H. & Mann, S. Bacterial templating of ordered macrostructures in silica and silica-surfactant mesophases. *Nature* **385,** 420–423 (1997).
18. Davis, S. A. *et al.* Brittle bacteria: A biomimetic approach to the formation of fibrous composite materials. *Chem. Mater.* **10,** 2516–2524 (1998).
19. Hopwood, J. D. & Mann, S. Synthesis of barium sulfate nanoparticles and nanofilaments in reverse micelles and microemulsions. *Chem. Mater.* **9,** 1819–1828 (1997).

Acknowledgements

We thank S. A. Davis for valuable discussions, the University of Bristol for a postgraduate scholarship to M.L., and the Max-Planck Society for financial support to H.S.

Correspondence and requests for materials should be addressed to S.M. (e-mail: s.mann@bris.ac.uk).